Vibrational Spectra of PtCO and $Pt(CO)_2$ Isolated in Solid Argon: Trends in Unsaturated Group 10 Metal Carbonyl Molecules†

Laurent Manceron,* Benoît Tremblay, and M. E. Alikhani

LADIR/Spectrochimie Moléculaire, UMR CNRS, Université Pierre et Marie Curie, Boîte 49, 4 Place Jussieu, 75252 Paris, Cedex 05, France

Received: November 2, 1999; In Final Form: January 20, 2000

The infrared spectrum of PtCO isolated in solid argon has been reinvestigated. Isotopic data on ν_1, ν_2, ν_3, $2\nu_1$, and $\nu_1 + \nu_3$ have been measured in the near- and far-infrared regions. This enables a complete harmonic force-field calculation based on a linear geometry, in agreement with all theoretical predictions. Comparisons of spectroscopic parameters for the NiCO, PdCO, and PtCO series experimental and theoretical binding energies are also presented. These results show that the perturbations of the CO ligand (CO bond force constants and ν_1 frequency shifts) are unreliable indicators of the evolution of the metal−ligand interaction energies, contrary to the metal−carbon force constant. Comparison with theoretical predictions of the fundamental frequencies indicates a systematic underestimation of the bending frequencies, especially sensitive for the heavy atom monocarbonyls. Similarly, the IR spectrum of $Pt(CO)_2$ has been studied, enabling the determination of the ν_1, ν_2, ν_3, ν_4, and ν_6 fundamentals of this molecule and a discussion of the evolution of the Pt−C and C≡O force constants with the coordination number. Complementary results concerning $Pt(CO)_n$ ($n = 3$, 4) are also presented.

Introduction

The importance of binary group 10 transition metal (TM) carbonyls in industrial processes, in catalysis, or as precursors for larger TM complexes has stimulated both theoretical and experimental studies. Although nickel carbonyl has been known and used for decades, the binary analogues of palladium and platinum have eluded direct synthesis at room temperature, presumably because of the unsufficient stability of the fully coordinated species.[1] Direct synthesis by metal atom and carbon monoxide co-deposition in cryogenic media has been applied early to this problem, and $Pd(CO)_4$ and $Pt(CO)_4$ have been synthesized at low temperature in solid rare gas[2−4] and characterized using vibrational spectroscopy. As in most vibrational studies of metal carbonyl compounds, conclusions were based on the analysis of the carbonyl stretching vibrations because of their easy detection due to exceptionally large transition moments[5,6] and because of the relative success of the energy-factored force-field approximations in giving the general outlines of the molecular shapes.[7,8] Because of the large body of data on the carbonyl stretching vibrations, these workers and others[9] tried to link the variation of the pseudodiatomic C≡O force constant to changes in the electronic structure or the metal−CO binding energy. If some empirical relationships enjoy a limited success within homologous series involving the same metal, it is obvious that they have no general predictive power. The $Ni(CO)_4$ and $Pt(CO)_4$ species, for instance, are reported to have similar pseudodiatomic C≡O force constant values[4] despite different stabilities.[10] Another simple example is given by comparison of the monocarbonyls of the neighboring Ni and Cu atoms, which have almost identical CO stretching frequencies (1996 cm^{-1} for NiCO[11] and 2010 cm^{-1} for CuCO[12]) despite very different binding energies[13,14] (41 and 6 kcal/mol, respectively). The lower frequency modes involving primarily the metal ligand stretching and bending coordinates are more direct markers of the interaction strength but are intrinsically weak and thus usually left aside in most studies, except in the comprehensive work of Jones on the coordinatively saturated species $Ni(CO)_4$, $Fe(CO)_5$, and $M(CO)_6$ (M = Cr, Mo, or W).[15]

Recently, we have shown that it is possible to obtain complete sets of vibrational data for the NiCO, CuCO, and PdCO triatomics isolated in solid argon and to derive Ni−C, Pd−C, and Cu−C force constants, which are much more directly related to the strength of the coordination,[16−18] and it is thus of interest to investigate the platinum analogue. Nickel, palladium, and platinum monocarbonyls have been the object of a large number of theoretical studies because they are considered important prototypes for modeling the coordination bonding mechanism onto TM. For these closed shell species, accurate modeling of the chemical bonding requires careful treatment of electron correlation and, for the heavier TM atoms, of the relativistic effects. Also, in contrast with lighter TM carbonyls, PtCO has been studied by a relatively limited number of theoretical techniques.[19−27] All these methods agree in predicting a linear, $^1\Sigma^+$ ground state (thus correlating with the Pt ^1S state, not the ^3D ground state), although they predict quite different binding energies (from 18 to 99 kcal/mol in the latest three studies[24−27]). In the more recent work of Chung et al.,[26,27] calculations on the monocarbonyls of Ni, Pd, and Pt have demonstrated how relativistic effects play an important role in the bonding description for the PtCO molecule and particularly affect some of the observables. The Pt−CO binding energy and the ν_3 vibrational frequency appeared to be the most sensitive to relativistic effects, but the deformation frequency, ν_2, was not calculated. If nearly all theoretical studies present relatively similar predictions on the upper frequency, ν_1 CO stretching mode, they differ significantly on the energies of the lower frequency metal−ligand vibrations. These are more sensitive

† Part of the special issue "Marilyn Jacox Festschrift".
* To whom correspondence should be addressed.

10.1021/jp9938819 CCC: $19.00
Published on Web 03/14/2000

markers of the description of the metal−ligand interaction as the normal coordinate associated to the vibration follows the reaction coordinate more closely. Such experimental results on these molecules are thus interesting to test the validity of these calculations.

In this study, we present an investigation of the low-frequency stretching and the bending modes of PtCO isolated in solid argon, as this information constitutes crucial testing grounds of the quality of the theoretical studies attempting to describe the Pt−CO bonding. Theoretical estimates of the vibrational harmonic frequencies will be presented and compared for the three monocarbonyls of the platinum triad.

In the course of these investigations, some discrepancies appeared with the attribution of the former workers concerning the identification of the high-frequency mode, ν_1, which must be clarified as a consequence, and new isotopic data on the CO stretching vibration and observations of overtone and combination binary levels in the near-infrared are reported here. A parallel study of $Pt(CO)_2$ enables assignment of ν_1, ν_2, ν_3, ν_4, and ν_6 of this molecule and a discussion of the evolution of the Pt−C and C≡O force constants with the coordination number. Although the experiments in this study were not designed to optimize the production of the $Pt(CO)_3$ and $Pt(CO)_4$ species, complementary information on these systems will be presented.

Experimental Section

Experimental procedures and methods were almost the same as those used in refs 16−18. The PtCO molecules were prepared by co-condensing Pt vapor and dilute CO−Ar mixtures (0.1−2% CO in Ar) onto a flat, highly polished, Ni-plated copper mirror maintained at less than 10 K using a closed-cycle cryogenerator, situated in a stainless steel cell evacuated at a base pressure less than 5×10^{-7} mbar before refrigeration of the sample holder. For this study, the furnace was modified to enclose the metal atom source inside a liquid nitrogen-cooled assembly; this minimized greatly the amount of outgassing impurities caused by the elevated temperature of the metal source. A tungsten filament, wetted with platinum (CFLA, France, 99.99%), was heated from 1700 to 2000 °C to generate the Pt vapor. The metal deposition rate was carefully monitored with the aid of a quartz microbalance and was typically of the order of about $4-50 \times 10^{-8}$ g/min.

High-purity argon (Prodair; 99.995%) and carbon monoxide (Matheson; 99.5%), ^{13}CO (CEA, Saclay, France; 99% ^{13}CO, including 9% $^{13}C^{18}O$) and $^{12}C^{18}O$ (MSD; 98% ^{18}O), were used to prepare the CO−Ar mixtures after removing condensable impurities with a liquid N_2 trap.

In general, after deposition times varied between 20 min and 2 h, infrared spectra of the resulting sample were recorded in the transmission−reflection mode between 5000 and 70 cm^{-1} using a Bruker 120 FTIR spectrometer and suitable combinations of CaF_2/Si, KBr/Ge, or 6-μm Mylar beam splitters with either liquid N_2-cooled InSb or narrow band HgCdTe photodiodes or a liquid He-cooled Si−B bolometer fitted with cooled band-pass filters. The resolution was varied between 0.05 and 0.5 cm^{-1}. Bare mirror backgrounds, recorded at 10 K from 5000 to 70 cm^{-1} prior to sample deposition, were used as references in processing the sample spectra. Also, absorption spectra in the near-, mid- and far-infrared were collected *on the same samples* through either CaF_2, CsI, or polyethylene windows mounted on a rotatable flange separating the interferometer vacuum (10^{-2} mbar) from that of the cryostatic cell (10^{-7} mbar). The spectra were subsequently subjected to baseline correction to compensate for infrared light scattering and interference patterns. For these kind of molecules, the IR intensity measurements required special attention, as the objects of study present both very strong and very weak absorptions and in different spectral domains. Care was taken first to make measurements on the same samples in the various spectral ranges; second, to repeat these measures on optically thin and thick samples to avoid large photometric errors; and last, to use the band decomposition procedure to estimate relative intensities for partially overlapping bands.

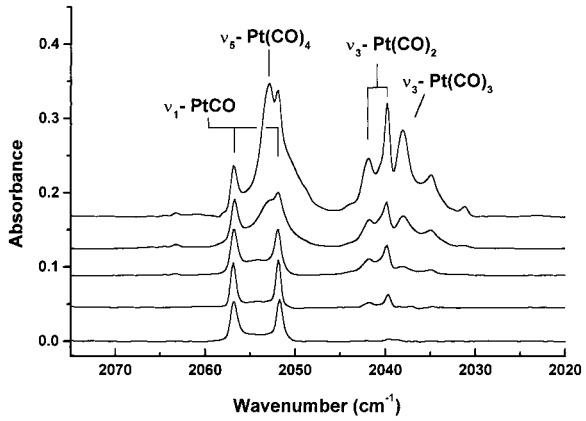

Figure 1. Infrared spectra of $Pt(CO)_n$ complexes in the CO stretching region: platinum and CO concentration study. From bottom to top: Pt/CO/Ar = 0.05/0.2/100; Pt/CO/Ar = 0.07/0.5/00, absorbance scale ×0.33; Pt/CO/Ar = 0.06/1/100, ×0.16; Pt/CO/Ar = 0.06/2/100, ×0.08; Pt/CO/Ar = 0.06/3.5/100, ×0.05. The absorbance scale for each spectrum is approximately normalized to the product of the reactant molar ratios.

The sample was next irradiated at 313 or 334 nm for approximately 30 min using a 200 W mercury−xenon high pressure arc lamp and an interference filter centered on the Hg emission line at 313 nm, as it was found that the object of study, the PtCO molecule, could be selectively partially destroyed by irradiation at this wavelength. Infrared spectra of the photolyzed samples were recorded between 5000 and 70 cm^{-1} as outlined above.

Results

Platinum vapor was first co-condensed with dilute mixtures of CO in argon (0.1−0.5/100) at 10 K to favor the formation of platinum monocarbonyl, PtCO. In the CO stretching region, the only spectral range covered in the earlier study, the products are very strongly absorbing, and the reactant concentrations can be varied over almost 2 orders of magnitude. Even for very diluted samples, two narrow absorptions (fwhm = 0.9 cm^{-1}) can be detected at 2056.8 and 2051.9 cm^{-1}, overlapping a broader, ill-defined one around 2054 cm^{-1}. These bands are always present as the main product when varying the Pt/Ar and CO/Ar molar ratios from 0.01 to 0.5%. They behave similarly upon sample annealing or irradiation and should thus be assigned to the lowest stoichiometry molecule containing one Pt atom and one CO molecule, PtCO, present in different trapping sites in the argon matrix. The existence of several, slightly different trapping sites will be confirmed on the other fundamental, harmonic, and combination transitions of this species. When the CO concentration was progressively augmented, other absorptions appeared, first at 2041.7−2039.8 and steadily increasing with the CO concentration, next at 2038, and finally at 2053 cm^{-1} (the latter species overlapping the PtCO multiplet) and increasing much faster with the CO concentration. These can be assigned to $Pt(CO)_2$, $Pt(CO)_3$, and $Pt(CO)_4$, respectively (see Figure 1). Kündig et al. had reported absorptions at 2052,

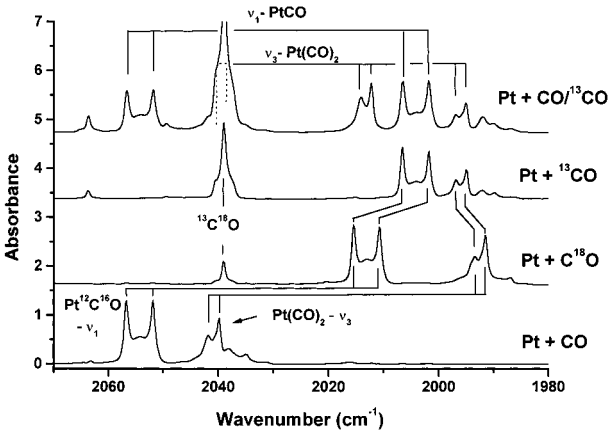

Figure 2. Infrared spectra of platinum carbonyl complexes in the CO stretching region for various isotopic precursors. From bottom to top: Pt + CO; Pt + $C^{18}O$; Pt + ^{13}CO; Pt + ($CO/^{13}CO$ = 1.1). The ^{13}CO sample contains about 8% $^{13}C^{18}O$ as isotopic impurity. In all samples, the Pt/CO/Ar molar ratio is approximately the same: 0.8/20/1000.

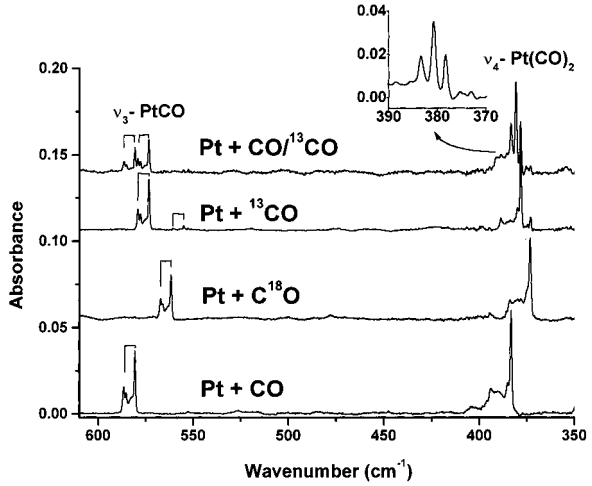

Figure 3. Infrared spectra of platinum mono- and dicarbonyl in the low-frequency stretching mode region for various isotopic precursors. From bottom to top: Pt + CO; Pt + $C^{18}O$; Pt + ^{13}CO; Pt + ($^{12}C^{16}O/^{13}C^{16}O$ = 1.1). The ^{13}CO sample contains about 8% $^{13}C^{18}O$ as isotopic impurity. In all samples, the Pt/CO/Ar molar ratio is approximately the same: 0.8/20/1000.

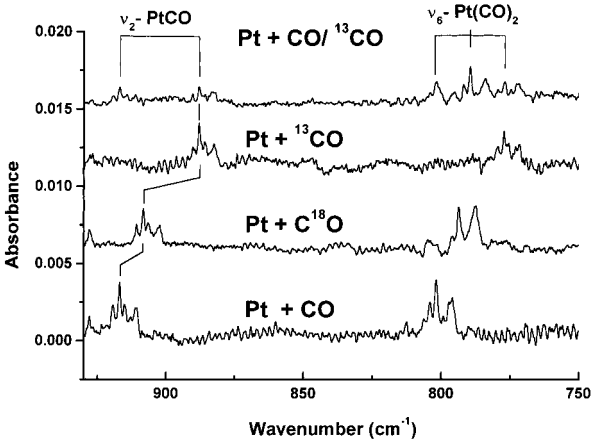

Figure 4. Infrared spectra of platinum mono- and dicarbonyl in the bending mode region for various isotopic precursors. From bottom to top: Pt + CO; Pt + $C^{18}O$; Pt + ^{13}CO; Pt + $CO/^{13}CO$. The Pt/CO/Ar molar ratio is approximately the same: 0.8/20/1000 for the pure isotope experiments and 0.8/40/1000 for the isotopic mixture.

2058, 2049, and 2053 cm^{-1} as belonging to PtCO, $Pt(CO)_2$, $Pt(CO)_3$, and $Pt(CO)_4$, respectively.[4] Apart from the broad absorption around 2053 cm^{-1} assignable to the final product of highest stoichiometry, $Pt(CO)_4$, the product identification must be revised accordingly. When either CO_2 or N_2 is added as ternary dopant in the samples, other bands appear that are also mentioned in ref 4 and should therefore correspond to ternary complexes.

Further evidence is provided by the isotopic effects (Figure 2). The PtCO multiplet corresponding to the carbonyl stretching mode, ν_1, presents very specific $^{12}C/^{13}C$ and $^{16}O/^{18}O$ isotopic shifts, different from that reported previously. The $^{12}C/^{13}C$ shift is noticeably larger than the $^{16}O/^{18}O$ shift (−50.2 vs −41.8 cm^{-1}) and different from the CO stretching of either the CO diatomics or the $Pt(CO)_2$ species. Also, in experiments run with $^{12}CO + ^{13}CO$ isotopic mixtures, the $Pt(CO)_2$ absorption produces a clear triplet pattern for $Pt(CO)_2$, $Pt(CO)(^{13}CO)$, and $Pt(^{13}CO)_2$, with an intermediate component at 2012.2 cm^{-1}, somewhat below the average of the isotopically pure species at 2039.8 and 1994.9 cm^{-1}, characteristic for a dicarbonyl species.

Several other new, weaker absorptions appeared in the far-, mid-, and near-infrared ranges (Figures 3−6). Among these, four multiplets near 580, 917, 2631, and 4080 cm^{-1} behaved as the strong PtCO ν_1 band after concentration changes or temperature and irradiation effects. All these absorptions also presented doublet patterns with $^{12}CO + ^{13}CO$ isotopic mixtures and thus belong to the PtCO molecule. Vibrational frequencies and relative intensities for all the observed isotopic species of PtCO are given in Table 1. Also, an estimate of the absolute intensities was possible here as, in diluted samples (Pt/CO/Ar ≅ 1/1/1000), it is possible to follow that, upon very mild warm-up of the polycrystalline argon matrix, the growth of PtCO correlated with the disappearance of the parent CO molecule before the formation of larger aggregates. From these measurements, a 11.5 ± 2.5 integrated intensity ratio can be derived between the ν_1 CO stretching vibration of PtCO and the CO diatomics fundamental, which yields an estimate of 700 ± 200 km/mol for this very strong band from known integrated intensities for the CO diatomics.[30]

Other new absorptions can be correlated with the $Pt(CO)_2$ IR-active CO stretching mode near 2040 cm^{-1}, also increasing with the CO concentration or when the sample is annealed, which are reported in Table 2. For all the absorptions near 4160, 2533, 802, and 383 cm^{-1}, characteric triplet patterns are observed using $^{12}CO + ^{13}CO$ isotopic mixtures (see, for instance, Figures 3 and 5−7), which clearly fingerprint these absorptions as belonging to the platinum dicarbonyl. Two very weak features observed at 2129.1 and 479.7 cm^{-1} are observed specifically in the isotopically mixed experiments. No absorption is observed in their vicinity when either CO or ^{13}CO isotopic precursor alone was used. Annealing the sample proved to be useful both to increase the amount of dicarbonyl and to reduce the spectral line widths. This was important in the study of the lower band near 380 cm^{-1}: the use of moderately high resolution (0.05 cm^{-1}) enables the detection of, for each trapping site absorption, a partially resolved quartet structure with approximately a 5/5/3.5/1 relative intensity pattern (Figure 7).

Although the study of larger carbonyl species was not the aim of the present study, several new bands have been detected for both $Pt(CO)_3$ and $Pt(CO)_4$ species, which are listed in Tables 3 and 4. The IR-active CO stretching mode for $Pt(CO)_3$ gives, using $^{12}CO + ^{13}CO$ isotopic mixtures, the characteristic quartet pattern as discussed in ref 29 by Darling and Ogden et al. for a D_{3h} trigonal planar species. No IR absorption is detected between the weak 2523.3 cm^{-1} transition and the strong 2040

TABLE 1: Vibrational Frequencies[a] and Relative Intensities of the IR Absorption Bands Observed for Various Species of PtCO

$Pt^{12}C^{16}O$		$Pt^{13}C^{16}O$	$Pt^{13}C^{18}O$	$Pt^{12}C^{18}O$	proposed assign.
4089.3		3989.7	no[b]	4007.4	$2\nu_1$
4084	[0.006][c]	3985		4003	
4079.0		*3979.9*		3998.7	
2642.2		2585.0	2512	2581.3	$\nu_1 + \nu_3$
2641.8	[0.007]	2583.6		2580.1	
2631.2		*2574.2*		*2571.0*	
2056.8		2006.6	1963.9	2015.5	ν_1
2054.3	[1]	2004.1	*1959.1*	2013.1	
2051.9		*2001.8*		*2010.8*	
919.4		890	no	910.7	ν_2
916.8	[0.0025]	*888.0*		*908.4*	
914.8		885.8		906.4	
911.0		882.5		902.6	
586.7		579.2	*555.1*	567.3	ν_3
585.4	[0.019]	577.9		566.1	
580.8		*573.4*		*561.8*	

[a] Vibrational frequencies in cm^{-1}. The values quoted are within ± 0.1 cm^{-1}, except for the integer values. The value of the main site is italicized. [b] Not observed. [c] Relative IR intensities with respect to ν_1. The ν_1 absolute IR intensity is estimated to be 700 ± 200 km/mol.

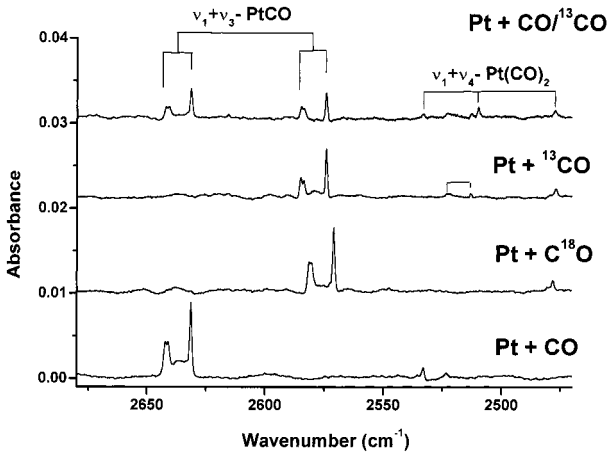

Figure 5. Infrared spectra of platinum mono- and dicarbonyl in the $\nu_1 + \nu_2$ (PtCO) and $\nu_1 + \nu_4$ ($Pt(CO)_2$) combination region for various isotopic precursors. From bottom to top: Pt + CO; Pt + $C^{18}O$; Pt + ^{13}CO; Pt + CO/^{13}CO.

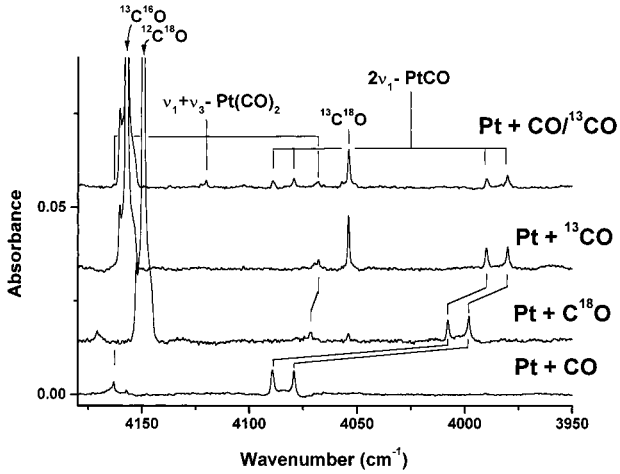

Figure 6. Infrared spectra of platinum monocarbonyl in the CO stretching overtone region for various isotopic precursors. From bottom to top: Pt + CO; Pt + $C^{18}O$; Pt + ^{13}CO; Pt + (CO/^{13}CO = 1.1). The ^{13}CO sample contains about 8% $^{13}C^{18}O$ as isotopic impurity. In all samples, the Pt/CO/Ar concentration is approximately the same (0.8/20/1000) but for the isotopic mixture (0.8/40/1000).

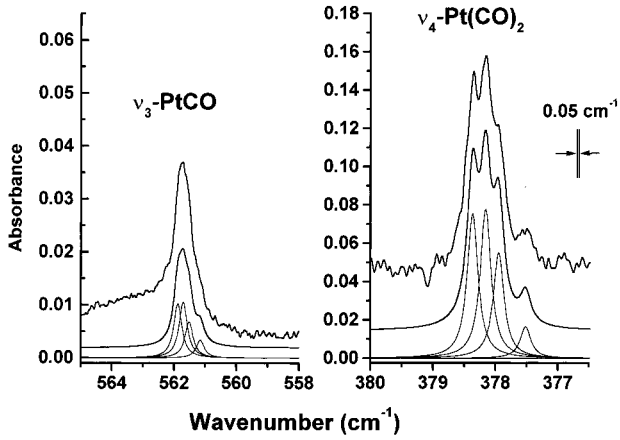

Figure 7. Comparison of high-resolution spectra of the main trapping site for ν_3 of PtCO (^{18}O-labeled) and ν_4 of $Pt(CO)_2$ (^{13}C-labeled) with simulations based on the harmonic force-field calculations presented in the text, the natural distribution of the $^{194}Pt/^{195}Pt/^{196}Pt/^{198}Pt$ platinum main isotopes, Lorentzian band shapes with 0.3 and 0.2 cm^{-1} line widths, respectively.

cm^{-1} band. Three low-frequency bands are detected near 486, 448, and 348 cm^{-1}, displaying very different $^{12}C/^{13}C$ and isotopic shifts but distinct quartet patterns using a $^{12}CO + ^{13}CO$ isotopic mixture. Our results for the CO stretching modes of $Pt(CO)_4$ are in agreement with those of Kündig et al.[4] The second strongest band of $Pt(CO)_4$ is observed at 311.3 cm^{-1}, presumably corresponding to the 304 cm^{-1} band mentioned in ref 4, and presents nearly identical $^{12}C/^{13}C$ and $^{16}O/^{18}O$ isotopic shifts. Unfortunately, the isotopic pattern is not clearly resolved in isotopically mixed experiments. Another absorption at 467

TABLE 2: Vibrational Frequencies[a] and Relative Intensities of the IR Absorption Bands Observed for Various Species of $Pt(CO)_2$

$Pt(^{12}C^{16}O)_2$		$Pt(^{12}C^{16}O)(^{13}C^{16}O)$		$Pt(^{13}C^{16}O)_2$	$Pt(^{12}C^{18}O)_2$	proposed assign.
4163.5	$[3.5 \times 10^{-3}]$[b]	4120.0	[0.001]	*4068.0*	*4071.8*	$\nu_1 + \nu_3$
4157.6						
2533.1	$[7.5 \times 10^{-3}]$	*2509.7*	[0.001]	*2477.0*	*2478.2*	$\nu_1 + \nu_4$
no[c]		*2129.1*	[0.02]	no	no	ν_1
2039.8	[1]	*2012.2*	[1]	1996.9	*1991.5*	ν_3
				1994.9		
801.9	$[5.8 \times 10^{-3}]$	*789.5*	[0.013]	779.5	796.1	
796.1				*777.2*	*793.8*	ν_6
				771.8	787.8	
no		479.7	$[1.5 \times 10^{-4}]$	no	no	ν_2
390	$[8.5 \times 10^{-2}]$	*380.8*	[0.086]	385	381	
383.4				*378.3*	*373.4*	ν_4

[a] Vibrational frequencies in cm^{-1}. The values quoted are within ± 0.1 cm^{-1}, except for the integer values. The value of the main site is italicized [b] Relative IR intensities with respect to ν_3. [c] Not observed.

TABLE 3: Vibrational Frequencies[a] and Relative Intensities of the IR Absorption Bands Observed for Various Species of $Pt(CO)_3$

$Pt(^{12}C^{16}O)_3$	$Pt(^{12}C^{16}O)_2{}^{13}C^{16}O$	$Pt^{12}C^{16}O(^{13}C^{16}O)_2$	$Pt(^{13}C^{16}O)_3$	$Pt(^{12}C^{18}O)_3$	proposed assign.
4158	no[b]	no	no	no	$\nu_1 + \nu_3$
2523.3	no	no	2464.2	2458.2	$\nu_1 + \nu_5$
2038.1	2001.8	2007	1992.1	1991.3	ν_3
485.8	484.4	479.7	473.2	478.1	ν_4
447.5	no	436.4	431.5	444.2	ν_5
348.5	346.2	344.2	341.7	341.3	ν_8

[a] Vibrational frequencies in cm^{-1}. The values quoted are within ± 0.1 cm^{-1}, except for the integer values. [b] Not observed.

TABLE 4: Vibrational Frequencies[a] and Relative Intensities of the IR Absorption Bands Observed for Various Species of $Pt(CO)_4$

$Pt(^{12}C^{16}O)_4$	$Pt(^{13}C^{16}O)_4$	$Pt(^{12}C^{18}O)_4$	proposed assign.
2519.9	2461.4	2457.6	$\nu_5 + \nu_6$
2431.5	2375.7	2378.7	$\nu_1 + \nu_7$
2053.0	2006.6	2006.2	ν_5
467.1	454.5	459.1	ν_6
311.3	305.0	305.5	ν_7

[a] Vibrational frequencies in cm^{-1}.

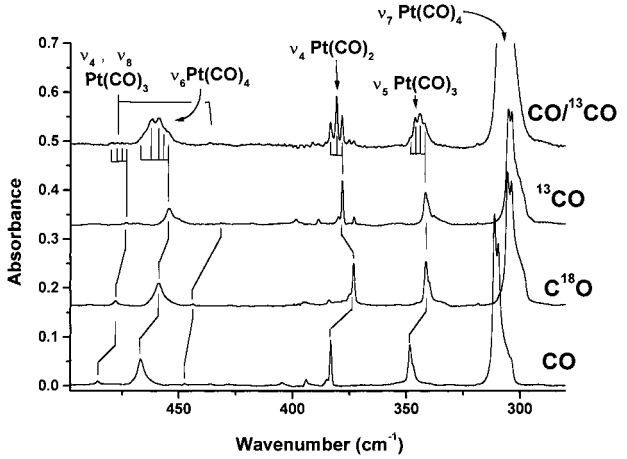

Figure 8. Infrared spectra of platinum di-, tri-, and tetracarbonyl in the low-frequency stretching mode region for various isotopic precursors. From bottom to top: Pt + CO; Pt + $C^{18}O$; Pt + ^{13}CO; Pt + ($^{12}C^{16}O/^{13}C^{16}O = 1.1$). The ^{13}CO sample contains about 8% $^{13}C^{18}O$ as isotopic impurity. In all samples the Pt/CO/Ar molar ratio is approximately the same: 0.8/20/1000.

cm^{-1} presents a larger $^{12}C/^{13}C$ than $^{16}O/^{18}O$ shift and a partially resolved quintet using a $^{12}CO + {}^{13}CO$ isotopic mixture (Figure 8).

Vibrational Analysis. *PtCO*. From the concentration and isotopic effects, the positions of five absorption bands belonging to PtCO have been clearly established, which means that at least two are either overtone or combination levels. Each absorption is split by the presence of multiple trapping sites in the argon matrix, an unfortunate situation often encountered in matrix-isolation studies, even for other, stable and well-known linear molecules such as CO_2.[31] Nevertheless, the influence of the matrix is presumably very small since the frequencies are close to each other and the measured isotope shifts are identical from one site to the next within experimental uncertainty. For the sake of clarity, the frequencies for the main trapping site will be used in the following modeling and discussion of the molecular properties. Assignment of the strong carbonyl stretching mode at 2051.9 cm^{-1}, ν_1, is straightforward, but the isotope effects deserve a few comments, as they differ qualitatively from those of an isolated CO oscillator. The $C^{16}O/C^{18}O$ and $^{12}CO/^{13}CO$ isotopic shifts for a pseudodiatomic at that frequency would be about 49.1 and 47.1 cm^{-1}, respectively, following the evolution of the reduced masses. If we define Δ as the difference between these two effects, this parameter thus goes from a 2 cm^{-1} positive value in a CO pseudodiatomics to -9 cm^{-1} for ν_1 of PtCO. This trend, already apparent in PdCO ($\Delta = -2.7$ cm^{-1})[18]and NiCO ($\Delta = -6.9$ cm^{-1}),[16] is even more pronounced in PtCO, indicative of a larger mechanical coupling between the M−C and C≡O coordinates, caused by a stronger coordination bond (vide infra).

The second strongest absorption is the lowest frequency band at 580.8 cm^{-1}, for which the $PtC^{16}O/PtC^{18}O$ effect is 2.5 times larger than the $Pt^{12}CO/Pt^{13}CO$ one, as expected for the remaining Σ^+ symmetry ν_3 stretching fundamental of a linear PtCO molecule, with an in-phase character for the Pt−C and C−O coordinates.

The third fundamental, the bending vibration, ν_2, should be in a symmetry class of its own, and the isotope effects can be estimated in a first approach using the geometry calculated in the most recent theoretical study of Chung et al.,[27] that is, $R_{Pt-C} = 1.74$ Å and $R_{CO} = 1.16$ Å. Specifically, substitution of the central carbon atom will cause a much larger shift than that of the terminal oxygen. This is what is observed for the 917 cm^{-1} band, with $PtC^{16}O-PtC^{18}O$ and $Pt^{12}CO-Pt^{13}CO$ isotopic shifts of -8.4 and -28.8 cm^{-1}, respectively, as compared with -10 and -28 cm^{-1} calculated in the harmonic approximation with the above-mentioned geometry. Note that a position above 900 cm^{-1} is a surprisingly high value in regard to the theoretical predictions placing the bending vibrations between 370 and 560 cm^{-1}, but this latter spectral region is not congested, and no absorption can be detected there within the sensitivity limit of our experimental setup (see Figure 3).

The band observed at 4079 cm^{-1} is consistent with a $2\nu_1$ overtone. For $Pt^{12}C^{16}O$, $2 \times \nu_1 = 2 \times 2051.9$ or 4103.8 cm^{-1}, which represents a $2X_{11}$ anharmonicity constant of -24.8 cm^{-1}, in line with the NiCO and PdCO values (-23.8 and -25.8 cm^{-1}, respectively). The $^{16}O/^{18}O$ and $^{12}C/^{13}C$ isotopic shifts support this attribution, being nearly twice those observed for the ν_1 fundamental.

The weak absorption at 2631.2 cm^{-1} is assigned to a $\nu_1 + \nu_3$ combination level, again from the near coincidence of the frequency with the sum of the fundamentals ($\nu_1 + \nu_3 = 2051.9 + 580.8 = 2632.7$) and of the $^{16}O/^{18}O$ and $^{12}C/^{13}C$ isotopic shifts with the sum of the corresponding shifts on the fundamentals. Unlike in NiCO and PdCO, the $\nu_1 + \nu_2$ combination level was not observed, but this transition was the weakest observed for these molecules, and the product concentration achieved in this case is about a factor of 2 lower. The corresponding X_{12} were -5.5 and -8.9 cm^{-1} for NiCO and PdCO, respectively. By analogy, and on the basis of the X_{11} and X_{13} observed here for PtCO, we can estimate a ν_1 harmonic frequency at 2087 ± 5 cm^{-1} to facilitate comparisons with ab initio predictions.

A harmonic force-field calculation was carried out using the experimental data presented in Table 1 and a starting linear geometry with $R_{Pt-C} = 1.74$ Å and $R_{CO} = 1.16$ Å. The best fit

TABLE 5: Comparison of the Experimental Frequencies and Calculated[a] Harmonic Frequencies for the Various Isotopic Species of PtCO

	$Pt^{12}C^{16}O$			$Pt^{13}C^{16}O$		$Pt^{13}C^{18}O$		$Pt^{12}C^{18}O$	
		calcd							
	exp	^{195}Pt	^{194}Pt	exp	calcd[b]	exp	calcd[b]	exp	calcd[b]
$\nu_1(\Sigma^+)$	2051.9	2051.91	2051.91	2001.8	2001.1	1959.1	1957.9	2010.8	2010.2
$\nu_2(\Pi)$	916.8	916.80	916.78	888.0	888.7	no[c]	877.5	908.4	905.9
$\nu_3(\Sigma^+)$	580.8	580.99	580.80	573.4	573.4	555.1	554.9	561.8	561.4

[a] The force constant giving the best fit of the experimental data are $F_{PtC} = 5.146$ mdyn Å^{-1}, $F_{CO} = 16.22$ mdyn Å^{-1}, $F_{PtC,CO} = 0.85$ mdyn Å^{-1}, $F_{PtCO} = 2.249$ mdyn Å rad^{-2}. [b] Frequencies calculated with the ^{195}Pt isotope. [c] Not observed.

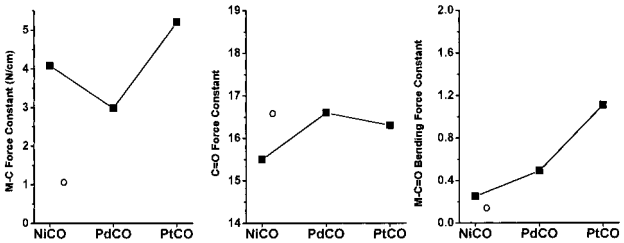

Figure 9. Comparison of the M−C, C≡O, and M−C≡O deformation (normalized to the bond lengths) harmonic force constants for the three group 10 triatomics (■) and, for comparison purposes, for the CuCO triatomics (○).

of the frequencies and isotope shifts is presented in Table 5, with a 0.27% standard deviation on the isotope shifts. Their simultaneous reproduction imposes severe constraints on the form of the normal coordinates, and in this case, all potential constants are relatively precisely determined. The reproduction of the isotope effects on the ν_1 and ν_3 stretching modes is very good, and the small discrepancies are well within the usual deviations due to anharmonicity. It confirms that the platinum isotope effects are well within the bandwiths ($\approx$0.3 cm^{-1}) for the two higher frequency vibrations, ν_1 and ν_2, and only participate in the line-broadening for the low-frequency stretching mode ν_3. (See the spectral simulation in Figure 7.) The deviations of the $^{12}C/^{13}C$ and $^{16}O/^{18}O$ isotope effects on the bending mode are a little larger and vary from one isotopic species to the other in different directions (+2.5 cm^{-1} with $PtC^{18}O$ and −0.7 cm^{-1} with $Pt^{13}CO$), regardless of the absolute magnitude of the shift. Such a situation was already noted for PdCO and, to a lesser extent, for NiCO. These small discrepancies could not be explained by anharmonicity effects. Other geometries were also tested, but since any departure from linearity resulted rapidly in a larger standard deviation, the molecule will be taken as linear. As discussed for PdCO, the fit also improves globally when shorter Pt−C and longer C−O distances are assumed, and this should indicate the direction in which modeling with more advanced ab initio techniques would result. Figure 9 presents the evolution of the main quadratic potential constants for the monocarbonyls of the nickel triad and of copper for comparison. Interestingly, the correlation between metal−carbonyl binding energies and carbonyl bond force constant variation is not even qualitative, but the metal−carbon force constants are a good quantitative indicator.

$Pt(CO)_2$. Platinum dicarbonyl has been supposed in earlier studies to have a linear shape[4,28] with $D_{\infty h}$ symmetry. For a penta-atomic species, one thus expects 10 normal modes and 7 distinct frequencies, of which only 4 are IR-active. These correspond to two Σ_u symmetry Pt−C and CO stretching and two Π_u symmetry Pt−C≡O and C−Pt−C bending vibrations. The latter motion is expected at very low frequency, and no suitable absorption has been detected in the present study down to 70 cm^{-1}. From the $PtC^{16}O/PtC^{18}O$ and $Pt^{12}CO/Pt^{13}CO$ isotopic shifts, assignments of the two strongest bands at 2039.8 and 383.4 cm^{-1} to the Σ_u symmetry vibrations, ν_3 and ν_4, are straightforward. Note that, as the ν_4 frequency decreases, the $PtC^{16}O/PtC^{18}O$ isotopic shift becomes larger than the $Pt^{12}CO/Pt^{13}CO$ one ($\Delta = +3.4$ cm^{-1} vs −8.9 in PtCO), as the coupling between the Pt−C and C−O coordinates is less important.

In annealed samples which present better defined features on the ν_4 absorptions, it was possible to resolve each site into a quartet, whose intensity pattern corresponds to the naturally occurring distribution of ^{194}Pt, ^{195}Pt, ^{196}Pt, and ^{198}Pt isotopes (Figure 7). In samples prepared with a $^{12}CO + {}^{13}CO$ isotopic mixture, weaker absorptions appeared in different spectral regions, namely, near 2129 and 480 cm^{-1}, where no equivalent IR absorptions are observed for $Pt(^{12}CO)_2$ or $Pt(^{13}CO)_2$ only, which is consistent with a slight IR activation of the symmetrical stretching vibrations (ν_1, ν_2) for the $Pt(^{12}CO)(^{13}CO)$ species. At higher frequencies above 2500 and 4100 cm^{-1}, weak bands corresponding to binary levels involving these fundamentals are observed (ν_1 and ν_3, ν_1 and ν_4), thus confirming these assignments. The X_{13} and X_{14} anharmonic corrections are thus of the order of −21.3 and −0.5 cm^{-1}, very close to the $Ni(CO)_2$ values,[32] thus placing the ν_1 and ν_2 levels near 2150 and 480 cm^{-1} with normal isotopes. For ν_1, the Δ parameter is again negative (−6.2 cm^{-1}), consistent with a higher frequency for ν_2 than for ν_4. Unlike for $Ni(CO)_2$, which has a bent C_{2v} symmetry structure and thus IR-active symmetrical stretching vibrations,[32] for $Pt(CO)_2$, the nonobservation of the ν_1 and ν_2 vibrations is convincing evidence that the molecule remains linear or so close to linearity that the difference is not detectable.

As in PtCO, a band is observed above 800 cm^{-1} with $PtC^{16}O/PtC^{18}O$ and $Pt^{12}CO/Pt^{13}CO$ isotopic shifts characteristic for a Pt−C≡O bending mode (−8.1 and −24.7 cm^{-1}, respectively), which is assigned to the ν_6, Π_u symmetry vibration. The other, Π_g symmetry Pt−C≡O bending mode, ν_5, is not observed, but we have an indication of a much lower frequency, considering the position of the $Pt(^{12}CO)(^{13}CO)$ only slightly above the average of the isotopically pure ν_6 frequencies.

To test these hypotheses and to quantify the evolutions of the molecular spectroscopic parameters with the increase in coordination number, we have also performed semiempirical force-field calculations, based on a $D_{\infty h}$ symmetry and geometrical parameters equivalent to those used for PtCO.The results obtained with the best set of potential constants are presented in Table 6. The reproduction of the isotopic effects is very good, and the model thus predicts the position of the ν_2 and ν_5 IR-silent vibrations near 484 ± 1 and 500 ± 30 cm^{-1}, respectively, for the normal isotopes. It also confirms that the fine structure observed for the ν_3 mode is due to the isotopic distribution of a single platinum atom, as shown in the spectral simulation (Figure 7).

It is interesting to comment briefly on the evolution of the force constants between the mono- and dicarbonyl of platinum and nickel.[32] Both the CO and M−C force constants are larger in PtCO as compared to NiCO, thus showing that strengthening

TABLE 6: Comparison of the Experimental Frequencies and Calculated[a] Harmonic Frequencies for the Various Isotopic Species of $Pt(CO)_2$

	$^{194}Pt(^{12}C^{16}O)_2$		$^{195}Pt(^{12}C^{16}O)_2$		$Pt(^{12}C^{16}O)(^{13}C^{16}O)$		$Pt(^{13}C^{16}O)_2$		$Pt(^{12}C^{18}O)_2$	
	exp	calcd	exp	calcd	exp	calcd[b]	exp	calcd[b]	exp	calcd[b]
ν_1	2149.7	2149.90	2149.7	2149.90	2129.1	2129.3	2098.7	2098.0	2104.9	2104.1
ν_3	2039.8	2039.93	2039.8	2039.93	2012.2	2011.8	1994.9	1994.2	1991.5	1991.2
ν_6	801.9	801.96	801.9	801.93	789.5	789.5	777.2	776.5	793.8	794.4
ν_2	no[c]	483.75	no	483.75	479.7	480.1	no	476.3	no	466.0
ν_4	383.55	383.56	383.33	383.34	380.8	380.5	378.3	378.1	373.4	373.0

[a] The force constant giving the best fit of the experimental data are $F_{PtC} = 2.959$ mdyn Å^{-1}, $F_{CO} = 17.61$ mdyn Å^{-1}, $F_{CO,CO} = 0.33$ mdyn Å^{-1}, $F_{PtC,PtC} = 1.075$ mdyn Å^{-1}, $F_{PtC,CO} = 0.75$ mdyn Å^{-1}, $F_{PtCO} = 1.15$ mdyn Å rad^{-2}, $F_{CPtC} = -0.2$ mdyn Å rad^{-2}, $F_{OCPt,\ OCPt} = 0.4675$ mdyn Å rad^2, $F_{OC,PtC} = -0.2$ mdyn Å rad^{-2}, $R_{PtC} = 1.73$ Å, $R_{CO} = 1.15$ Å, $\alpha_{CPtC} = 180°$, $\theta_{PtCO} = 180°$. [b] Frequencies calculated with the ^{195}Pt isotope. [c] Not observed.

the coordination is not always linked to a weakening of the CO bond. The addition of a second ligand induces a weakening of the metal−carbon force constants for both metals but not in the same proportion. It decreases from 4.07 in NiCO to 2.8 mdyn Å^{-1} in $Ni(CO)_2$ (−31%) and drops more sharply from PtCO to $Pt(CO)_2$ (5.15 to 2.96 mdyn Å^{-1}, −43%). The variations of the CO bond force constant, on the other hand, are not in the inverse proportions (from ≈18.5 in CO to 15.44 and 16.28 in NiCO and $Ni(CO)_2$ but only to 16.22 and 17.61 mdyn Å^{-1} in PtCO and $Pt(CO)_2$, respectively).

$Pt(CO)_3$ and $Pt(CO)_4$. Unfortunately, the experimental data presented here for $Pt(CO)_3$ and $Pt(CO)_4$ are too incomplete to enable a similar quantitative treatment. Only a few facts can be briefly summarized. For $Pt(CO)_3$, the weak bands at 4158 and 2523 cm^{-1} are straightforward to assign to combinations involving the totally symmetric CO stretching mode with the degenerate, IR-active CO and Pt−CO stretching fundamentals near 2038 and 349 cm^{-1}. This places the IR-silent A'_1 symmetry CO stretching around 2176 ± 2 cm^{-1}. Since no absorption is detectable in this region, this represents very convincing evidence that $Pt(CO)_3$ is indeed trigonal planar. The bands observed near 486 and 448 cm^{-1} have unambiguous bending mode character, judging from the relative magnitudes of the $PtC^{16}O/PtC^{18}O$ and $Pt^{12}CO/Pt^{13}CO$ isotopic shifts (the latter is markedly larger than the former). The 486 cm^{-1} band is more likely the E' symmetry bending, coupled with the other E' symmetry stretching mode at 348.5 cm^{-1}, since their corresponding isotope effects are indicative of coupling between bending and stretching coordinates. On the other hand, the absorption at 447.5 cm^{-1} is likely the A_2'' symmetry, out-of-plane motion, as its isotope shifts are very close to those expected for a pure bending motion. Unfortunately, the remaining A_1' symmetry stretching could not be located, therefore preventing an estimate of the Pt−C force constant in the tricarbonyl.

For $Pt(CO)_4$, which is supposed to be of T_d symmetry, the position of the highest fundamentals, the A_1 symmetry CO stretching, ν_1, at 2119 cm^{-1} and the F_2 triply degenerate, ν_5, at 2053 cm^{-1} are known from previous Raman and IR experiments.[4] The other IR-active F_2 motions ν_6 and ν_7 are observed near 467 and 311 cm^{-1} in these experiments. Note that the upper 467 cm^{-1} band has again a marked bending mode character and is about 150 cm^{-1} higher in energy than the stretching vibration near 311 cm^{-1}. In $Ni(CO)_4$, the two corresponding vibrations were very nearly degenerate at 465 and 433 cm^{-1} in the same matrix-isolation conditions. The metal mass effect is much more sensitive on ν_7 than on ν_6 and accounts for roughly 70 cm^{-1} of the frequency decrease, the rest being due to change in the potential. The predictions of Jonas and Thiel[33] are indeed in very good agreement, thus showing that the approach used by these authors (gradient-corrected density functional, combined with quasi-relativistic effective core potential) seems effective for modeling the completely coordinatively saturated species.

Theoretical Calculations. Several theoretical studies have attempted to predict and describe the electronic structure and bonding in the PtCO triatomics. These are Hartree−Fock calculations by Gavezotti et al.[22,23] and Bash,[20] small multiconfigurations SCF−CI calculations by Bash and Cohen,[19] Moller−Plesset second-order perturbation theory of Rohlfing and Hay,[21] generalized valence bond calculations by Smith and Carter,[24] complete active space multiconfiguration SCF by Roszak and Balasubramanian,[25] and scalar relativistic density functional calculations with linear combination of Gaussian-type orbitals by Chung et al.[26,27] The results from the above studies show little agreement among the various calculations, demonstrating the sensitivity of this difficult system to the technique employed. Also, the dispersion in basic methods, the differences in basis sets, or the occasional use of different effective core potentials (ECP) makes it even more difficult to compare results obtained with other members of the platinum triad. Chung et al. performed such a systematic study but limited their frequency calculations to pseudodiatomic calculations on the stretching modes of the NiCO, PdCO, and PtCO triatomics using Xα and VWN functionals.[26,27] These authors analyzed thoroughly the importance of trends in the predicted electronic structure in the group 10 monocarbonyls (decomposing the relative weights of polarization, Pauli repulsion, π back-bonding, and σ donation contributions to the total binding energy) and also detailed the contribution of relativistic effects. Their main result was the prediction of a very amonotonic behavior along the series, with a M−CO binding energy decreasing from Ni to Pd but strongest with Pt (Table 7). The variation of the M−C bond force constant deduced here from experimental data confirms very nicely these theoretical predictions. The variations of the CO bond force constant, whose decrease has often been linked to the coordination binding energy, is not so clear to analyze. As discussed at length in refs 27 and 37, the variation of the CO bond force constant results mainly from two contributions of opposite effects: the Pauli repulsion, which increases the frequency (the role of σ donation being only of minor importance), and the π back-donation, which lowers the frequency. Chung et al. pointed out the large impact of relativistic effects on this last contribution for PtCO as a consequence of the contraction of the metal−carbon distance.[27] This should lead to smaller CO and larger M−C bond force constants in PtCO than in NiCO. If this is observed for the M−C bond parameter, the CO bond force constant does not follow that trend. Apparently, the decrease due to π back-donation must be more than offset by a Pauli repulsion and σ donation increase.

In papers on the larger carbonyl species, Li et al.[10] tested various quasi-relativistic corrections induced directly on the

TABLE 7: Comparison of Some Experimental Properties of PtCO with Calculated Values by a Number of Quantum Mechanical Methods[a]

	experimental			theoretical							
	NiCO	PdCO	PtCO	NiCO	PdCO	PtCO					
ν_1[b]	1994.5	2044.2	2051.9								
ω_1	2029 ± 1	2080 ± 1	2087 ± 5	1980	2026	2047	2042	2124	2119	2051	2085
ν_2	409.1	615.7	916.8								
ω_2				483	294	441	429	415	395		
ν_3	591.1	472.4	580.8								
ω_3				691	503	636	618	565	577	458	680
F_{CO} (mdyn Å^{-1})	15.44	16.57	16.22	14.3	16.2	15.8	15.9	17.4	17.4		
F_{MC} (mdyn Å^{-1})	4.07	2.98	5.15	5.9	3.4	6.3	5.9	4.9	5.1		
F_{MCO} (mdyn Å rad^{-2})	0.49	1.02	2.25	0.60	0.24	0.52	0.49	0.46	0.43		
R_{CO} (Å)				1.177	1.153	1.160	1.159	1.147	1.150	1.15	1.16
R_{MC} (Å)				1.631	1.833	1.753	1.757	1.792	1.787	1.93	1.74
binding energy[c]	41 ± 6[d]			84.5	43.5	77.6	78.1	66.4	66.3	52.8	98.9
theoretical method				MP2/LanL2DZ			MP2/Stoll	QCISD/Stoll	B3LYP/Stoll	DF(nrel)	DF(rel)
ref	16	18	*g*	*g*	*g*	*g*	*g*	*g*	*g*	26[e]	26[f]

[a] Comparison with different experimental and calculated data for NiCO and PdCO are also given. [b] Vibrational frequencies in cm^{-1}. [c] Binding energies (in kcal/mol) computed for ^{3}D state for Ni and Pt and ^{1}S for Pd. [d] Experimental value, ref 13. [e] Nonrelativistic calculations with binding energy computed for ^{1}S. [f] Relativistic calculations. [g] This work.

Hamiltonian in density functional calculations, while Jonas and Thiel[33,34] used classical gradient-corrected calculations but tested different ECP. This latter work demonstrated a relative success for such a cost-effective method and could be compared to the results of Frenking and coworkers with post-HF methods.[35,36] To test this latter approach on the smaller molecules of the platinum triad monocarbonyls and their performance for the reproduction of vibrational frequencies, we have carried out density functional MP2 calculations and added for PtCO a high level CI variational calculation with the same core potential and basis sets. The results are compared in Table 7 to experimental data and to the benchmark predictions of Chung et al.[26,27] Our goal here was 2-fold: to check whether it is possible to follow, using the ECP methods, the relationships existing between coordination energies and spectroscopic bond force constant parameters, and next, since our experimental results for NiCO, PdCO, and PtCO demonstrate a steady increase in the bending mode frequency with the heavier TM, whether it can be reflected using those modeling techniques.

All ab initio calculations were carried out using the Gaussian 98 quantum chemical package.[38] First, DF calculations were performed with the HF-DFT hybrid approach combining Becke's gradient-corrected exchange functional[39] with the correlation function of Lee et al.,[40] denoted as B3LYP. Second, calculations were carried out at the MP2 level. We have used for carbon and oxygen the 6-311 + G(2d)[41] and for the metal either the Los Alamos ECP[42] for core electrons plus double-ζ quality on valence electrons or the Stuttgart pseudopotential[43] (ECP2), with explicit treatment of the 18 valence electrons (for instance, for Pt (8s7p6d)/[6s5p3d]-Gaussian-type orbitals). The results with MP2/ECP1 and ECP2 and QCISD and DF-B3LYP/ECP2 are presented in Table 7. The trends calculated with DF-B3LYP on binding energies (D_e), bond distances, and stretching mode energies are consistent with the results of Chung et al.[26] except for an exaggerated stability for the Pd−CO binding energy. With MP2/ECP1 or ECP2, the trend is better reproduced but in the order $D_{NiCO} > D_{PtCO} \gg D_{PdCO}$, thus with an underestimated stability for PtCO versus NiCO. For both methods, the metal−carbon bond distances vary in the order Ni−CO ≥ Pt−CO > Pd−CO.

The evolution of the C≡O and M−C bond force constants is in qualitative agreement with the experimental values. The evolution of the C≡O force constants presents no qualitative correlation to the metal−CO binding energies at the difference of the M−C force constants. At all levels of calculations performed here (MP2 or DF, with either ECP methods), the predicted bending frequencies are systematically underestimated. If the error represents only 15% for NiCO, it is alarmingly large for PdCO and PtCO (by a factor 2.4, approximately). So, when comparing the predicted frequencies with the experimental data, the observed trend (ν_2 PtCO > ν_2 PdCO > ν_2 NiCO) is not reproduced, and the frequencies are very largely underestimated for the heavy atom systems; without that we could offer a simple explanation. Given the relative success of this approach in the work of Jonas and Thiel,[33,34] it seems that the shorter metal−carbon distance of the monocarbonyl poses a specific challenge for the treatment of relativistic effects, which cannot be specifically dealt with using ECP corrections. Higher frequencies for metal−ligand bending versus stretching modes had been observed and discussed for large, completely saturated TM carbonyl complexes[15,44] or large size saturated heme−CO systems,[45] but these situations are different and were largely attributed to steric or bonding considerations linked to the existence of a full coordination sphere, as opposed to the trends predicted in systematic studies for first row TM monocarbonyls.[46−50]

Conclusions

The infrared absorption spectrum of platinum monocarbonyl, synthesized by co-deposition of ground-state platinum atoms and carbon monoxide molecules in solid argon, has been measured. Data in the far-, mid-, and near-infrared range pertaining to isotopic species obtained with $^{12}C/^{13}C$ and $^{16}O/^{18}O$ substitutions have enabled assignments of all fundamental vibrations and of overtone and combination levels and are analyzed with the help of quadratic force-field calculations. IR absorption spectra were also obtained for $Pt(CO)_2$, relative to five fundamentals and two combinations for several isotopic species, and analyzed in a comparable framework. These models are of interest to discuss the strength of the TM−ligand bond and are important to compare the true quadratic force constants with the popular approximate pseudodiatomic or energy-factored treatments.[4,7,8] These results confirmed that these molecules are linear, or very close to linear, and are compared with theoretical predictions of the molecular properties and to results obtained for the nickel and palladium analogues. The predicted binding

energies in the relativistic calculations of Chung et al.[26,27] correlate well with the evolution of the metal−carbon bond force constant ($F_{PtC} > F_{NiC} > F_{PdC}$) but not with that of the CO ligand. Nevertheless, comparisons with previous and present theoretical predictions methods indicate that the evolution of the molecular energy upon bending seems at variance with experimental data. The deviations, small with nickel, are increasingly large with palladium and platinum. Calculations performed using ECP do not seem to reflect the observed trends for the monocarbonyl as accurately as for the completely coordinated species. The contraction due to relativity when going from Ni to Pt is probably much more sensible on the shorter coordination bond of the monocarbonyl species than on the longer one of the fully coordinated species. Comparing our experimental results for PtCO and $Pt(CO)_2$, the drop in the metal−carbon force constant observed here is larger than going from NiCO to $Ni(CO)_2$ and should be paralleled to (1) the differences in molecular shapes and electronic structures (linear for $Pt(CO)_2$, bent around the metal for $Ni(CO)_2$) and (2) the lack of stability of platinum versus nickel tetracarbonyl, despite a predicted greater binding energy in PtCO than in NiCO.

References and Notes

(1) *Comprehensive Organometallic Chemistry II*; Abel, E., Stone, F., Wilkinson, G., Eds.; Pergamon Press: Oxford, 1995; Vol. 9, Chapters 4 and 7.

(2) Darling, J. H.; Ogden, J. S. *Inorg. Chem.* **1971**, *11*, 666.

(3) Darling, J. H.; Ogden, J. S. *J. Chem. Soc., Dalton Trans*. **1973**, 1079.

(4) Kündig, E. P.; McIntosh, D.; Moskovits, M.; Ozin, G. A. *J. Am. Chem. Soc.* **1973**, *95*, 7234.

(5) Kettle, S. F.; Paul, I. *Adv. Organomet. Chem.* **1972**, *10*, 199.

(6) Bigorgne, M. *Spectrochim. Acta* **1976**, *32A*, 673.

(7) Cotton, F. A.; Kraihanzel, C. S. *J. Am. Chem. Soc.* **1962**, *84*, 4432.

(8) Braterman, P. S. *Metal Carbonyl Spectra*; Academic Press: New York, 1975.

(9) Timney, J. A. *Inorg. Chem*. **1979**, *18*, 2502.

(10) Li, J.; Schreckenbach, G.; Ziegler, T. *J. Am. Chem. Soc.* **1995**, *117*, 486.

(11) DeKock, R. L. *Inorg. Chem*. **1971**, *10*, 1205.

(12) Huber, H.; Kundig, E. P.; Moskovits, M.; Ozin, G. A. *J. Am. Chem. Soc*. **1976**, *97*, 2097.

(13) Sunderlin, L. S.; Wang, D.; Squires, R. R. *J. Am. Chem. Soc*. **1992**, *114*, 2788.

(14) Blitz, M. A.; Mitchell, S. A.; Hackett, P. A. *J. Phys. Chem*. **1991**, *95*, 8719.

(15) Jones, L. H. *Inorganic Vibrational Spectroscopy*; Marcel Dekker: New York, 1971; Vol. 1.

(16) Joly, H. A.; Manceron, L. *Chem. Phys.* **1998**, *226*, 61.

(17) Tremblay, B.; Manceron, L. *Chem. Phys*. **1999**, *242*, 235.

(18) Tremblay, B.; Manceron, L. *Chem. Phys.* **1999**, *250*, 187.

(19) Basch, H.; Cohen, D. *J. Am. Chem. Soc.* **1983**, *105*, 3856.

(20) Basch, H. *Chem. Phys. Lett*. **1985**, *116*, 58.

(21) Rohlfing, C. M.; Hay, P. J. *J. Chem. Phys*. **1985**, *83*, 4641.

(22) Gavezzotti, A.; Tantardini, G. F.; Simonetta, M. *Chem. Phys. Lett.* **1986**, *129*, 577.

(23) Gavezzotti, A.; Tantardini, G. F.; Miessner, H. *J. Phys. Chem.* **1988**, *92*, 872.

(24) Smith, G. W.; Carter, E. A. *J. Phys. Chem.* **1991**, *95*, 2327.

(25) Roszak, S.; Balasubramanian, K. *J. Phys. Chem.* **1993**, *97*, 11238.

(26) Chung, S.-C.; Krüger, S.; Pacchioni, G.; Rösch, N. *J. Chem. Phys.* **1995**, *102*, 3695.

(27) Chung, S.-C.; Krüger, S.; Ruzankin, S. P.; Pacchioni, G.; Rösch, N. *Chem. Phys. Lett*. **1996**, *109*, 248.

(28) Su, M.-D.; Chu, S.-Y. *Inorg. Chem*. **1998**, *37*, 3400.

(29) Darling, J. H.; Ogden, J. S. *J. Chem. Soc., Dalton Trans.* **1972**, 2496.

(30) Bishop, D. M.; Cheung, L. M. *J. Phys. Chem. Ref. Data* **1982**, *11*, 121.

(31) Freidin, L.; Nelander, B.; Ribbegard, G. *J. Mol. Spectrosc*. **1974**, *53*, 410

(32) Manceron, L.; Alikhani, M. E. *Chem. Phys.* **1999**, *228*, 73.

(33) Jonas, V.; Thiel, W. *J. Chem. Phys.* **1995**, *102*, 8474.

(34) Jonas, V.; Thiel, W. *J. Phys. Chem. A* **1999**, *103*, 1381.

(35) Dapprich, S.; Ehlers, A. W.; Frenking, G. *Chem. Phys. Lett.* **1995**, *242*, 521.

(36) Ehlers, A. W.; Frenking, G. *Organometallics* **1995**, *14*, 423.

(37) Bagus, P. S.; Hermann, K.; Bauschlicher, C. W., Jr. *J. Chem. Phys.* **1984**, *80*, 4378.

(38) Frisch, M. J.; Trucks, G. W.; Schlegel, H. B.; Gill, P. M. W.; Johnson, B. G.; Robb, M. A.; Cheeseman, J. R.; Keith, T. A.; Petersson, G. A.; Montgomery, J. A.; Raghavachari, K.; Al-Laham, M. A.; Zakrzewshi, V. G.; Ortiz, J. V.; Foresman, J. B.; Cioslowski, J.; Stefanov, B. B.; Nanayakkara, A.; Challacombe, M.; Peng, C. Y.; Ayalas, P.Y.; Chen, W.; Wong, M. W.; Andres, J. L.; Replogle, E. S.; Martin, R. L.; Fox, D. J.; Binkley, J. S.; DeFrees, D. J.; Baker, J.; Stewart, J. P.; Head-Gordon, M.; Gonzalez, C.; Pople, J. A. *Gaussian 98*; Gaussian, Inc.: Pittsburgh, PA, 1999.

(39) Becke, A. D. *J. Chem. Phys.* **1993**, *98*, 5648.

(40) Lee, C.; Yang, W.; Parr, R. G. *Phys. Rev. B* **1988**, *37*, 785.

(41) Frisch, M. J.; Pople, J. A.; Binkley, J. S. *J. Chem. Phys.* **1984**, *80*, 3265.

(42) Hay, P. J.; Wadt, W. R. *J. Chem. Phys.* **1985**, *82*, 270, 284, 299.

(43) Andrae, D.; Haeussermann, U.; Dolg, M.; Stoll, H.; Preuss, H. *Theor. Chim. Acta* **1990**, *77*, 123.

(44) Jones, L. H.; Swanson, B. I. *Acc. Chem. Res.* **1976**, *9*, 128.

(45) Pápai, I.; Stirling, A.; Mink, J.; Nakamoto, K. *Chem. Phys. Lett.* **1998**, *287*, 531.

(46) Bauschlicher, C. W., Jr.; Langhoff, S. R.; Barnes, L. A. *Chem. Phys*. **1989**, *129*, 431.

(47) Blomberg, M. R. A.; Sieghbahn, P. E. M.; Lee, T. J.; Rendel, A. P.; Rice, J. F. *J. Chem. Phys.* **1991**, *95*, 5898.

(48) Sodupe, M.; Bauschlicher, C. W., Jr.; Lee, T. J. *Chem. Phys. Lett.* **1992**, *189*, 266.

(49) Fournier, R. *J. Chem. Phys*. **1993**, *99*, 1801.

(50) Adamo, C.; Lelj, F. *J. Chem. Phys*. **1995**, *103*, 10605.